Applied Energy 211 (2018) 318–333

Contents lists available at ScienceDirect

Applied Energy

journal homepage: www.elsevier.com/locate/apenergy

Numerical simulation of aqueous ammonia-based CO_2 absorption in a sprayer tower: An integrated model combining gas-liquid hydrodynamics and chemistry

Yin Xu[a,b,*], Baosheng Jin[b], Yongling Zhao[a,c], Eric J. Hu[d], Xiaole Chen[b], Xiaochuan Li[a]

[a] School of Hydraulic, Energy and Power Engineering, Yangzhou University, Yangzhou 225127, Jiangsu, China
[b] Key Laboratory of Energy Thermal Conversion and Control of Ministry of Education, School of Energy and Environment, Southeast University, Nanjing 210096, Jiangsu, China
[c] School of Civil Engineering, The University of Sydney, Sydney, NSW 2006, Australia
[d] School of Mechanical Engineering, The University of Adelaide, Adelaide, SA 5005, Australia

HIGHLIGHTS

- A model integrating hydrodynamics and chemistry of NH_3-CO_2-H_2O system is developed.
- CO_2 removal efficiency and NH_3 escape are studied experimentally and numerically.
- Model using Liu's kinetics presents a better agreement with the experiments.
- Distribution of gaseous species and temperature depends on gaseous velocity field.
- Alternation of CO_2 removal efficiency at 303 K is observed and explained.

ARTICLE INFO

Keywords:
Post-combustion CO_2capture
Aqueous ammonia-based CO_2capture
CFD
Multiphase
Spray tower

ABSTRACT

CO_2 capture in the spray tower using aqueous ammonia solution has been proved a potential approach for the post-combustion CO_2 capture. To improve the performance of spray absorption, a new three-dimensional numerical model integrating the complex gas-liquid hydrodynamics and the chemistry of the NH_3-CO_2-H_2O system has been proposed and developed in this paper. In the model, the gas-liquid hydrodynamics was simulated using the Euler-Lagrange method, while the chemistry of the NH_3-CO_2-H_2O system, including both thermodynamic and kinetic characteristics, was modeled using user-defined modules implemented in the CFD package. Moreover, a laboratory scale spray absorption system was built, and run under various operating conditions were carried out in order to validate the model developed. Subsequently, the predicted results using different kinetic models were compared with the experimental results. It was found the model using Liu's kinetics showed a better agreement with the experiments, especially when the liquid temperature and NH_3 concentration of solution vary. Furthermore, the validated model was used to study the fundamentals of spray absorption. It has been found that the gas temperature profile as well as gaseous CO_2 and NH_3 concentration profile depends on the velocity field, indicating the hydrodynamics should be considered when optimizing the design of reactor. It has also been found that the residence time of droplets increases with the increase of gas flow rate, leading to an increase in average droplets temperature and CO_2 loading, while the increase of ammonia concentration of solution could significantly improve the overall CO_2 mass transfer coefficient. When the solution temperature increases from 293 K to 303 K, the overall CO_2 mass transfer coefficient gradually increases, resulting in CO_2 removal efficiency improvement. However, when the solution temperature increases from 303 K to 313 K, the promotion of reverse reaction leads to the reduction of CO_2 removal efficiency. In addition, the increase of ammonia solution flow rate would mainly increase the interphase area and promote both CO_2 absorption and NH_3 escape. The model developed in this paper can be used to optimize the design and operation of such reactors in practice.

Abbreviations: CFD, computational fluid dynamics; CSIRO, Australia's commonwealth scientific and industrial research organization; E-NRTL, the electrolyte nonrandom two-liquid model; IPCC, the intergovernmental panel on climate change; RNG, the renormalization group theory

* Corresponding author at: School of Hydraulic, Energy and Power Engineering, Yangzhou University, Yangzhou 225127, Jiangsu, China.
E-mail addresses: 006307@yzu.edu.cn (Y. Xu), bsjin@seu.edu.cn (B. Jin).

https://doi.org/10.1016/j.apenergy.2017.11.054
Received 10 June 2017; Received in revised form 17 October 2017; Accepted 7 November 2017
Available online 15 November 2017
0306-2619/ © 2017 Elsevier Ltd. All rights reserved.

1. Introduction

Research and development of CO_2 capture and storage (CCS) technologies are of great urgency and utmost importance for relieving environmental issues such as global warming, sea level rise, coastal region erosion, and abnormal climate [1–3]. According to a variety of reports, fossil-fuel combustion is a major contributor of anthropogenic CO_2 emissions, particularly coal combustion for electricity generation [4–7]. Therefore, over the past few decades, mitigating CO_2 emissions from thermal power plants have become popular topics and several technical options have been proposed, including post-combustion capture, pre-combustion capture, oxyfuel combustion, and chemical looping [8–11]. Among these alternatives, post-combustion capture (PCC) can be installed directly to existing plants, exhibiting an attractive economical advantage, which can also accelerate the implementation of CCS [12–17]. Previous studies on PCC widely used an aqueous monoethanolamine (MEA) solution as CO_2 absorbent [18–21]. However, the issues of high regeneration energy, easy degradation by SO_2 and O_2, and facilities corrosion, are always accompanied with the utilization of MEA [22]. As a promising alternative, an aqueous ammonia solution has been proposed due to the advantages of high capacity, low cost, less corrosion, low regeneration energy, no degradation in the presence of O_2 and SO_2, and the potential of removing CO_2, NO_x, and SO_2 simultaneously [23–25]. Consequently, ammonia-based CO_2 capture has been extensively studied in recent years. The thermodynamic data and models of NH_3-CO_2-H_2O system have been upgraded [26–28]. The kinetics of CO_2 absorption into ammonia aqueous solution has also been discussed thoroughly [29–38]. Pilot plants have been built to demonstrate the technical and economical feasibility of ammonia-based CO_2 capture by Alstom [39], Powerspan [40], and CSIRO [41,42], respectively. In the mean time, process simulation has been carried out to evaluate the performance of ammonia-based CO_2 capture [43–48]. Through these efforts, the technical feasibility of ammonia-based CO_2 capture has been successfully proven, which could achieve 90% CO_2 removal efficiency and 99% purity of product CO_2 [49]. However, special consideration should be paid to the issue of ammonia escape, which may result in ammonia loss and secondary pollution. That also hinders the industrial application of ammonia-based CO_2 capture [50]. For the worse, solid precipitation due to the reaction of escaped ammonia and CO_2 could cause plugging of pipes and valves, leading to a shutdown of the whole system [42].

Measures of installing additional washing system and cooling down the flue gas have been proposed to control ammonia escape [51,52]. However, these measures consume extra power and water, lowering the economical feasibility of ammonia-based CO_2 capture. Therefore, adding functional additives into the solution becomes another way of inhibiting ammonia escape. Various additives have been tested in labs, including hindered amines [53], alcohols [54], metal cations [55–57], and ionic liquids [58]. However, experimental results indicate that most additives have negative influence on CO_2 capture. Suitable additives are not yet available.

CO_2 absorption and ammonia escape are also influenced by reactor configuration and operating conditions. Thus, optimizing design of a reactor and its operating conditions can provide a potential solution to abovementioned issues. Over the past few years, ammonia-based CO_2 capture using packed columns has been studied extensively [59,60]. Especially, a rotating packed column has been proposed to intensify multiphase transportation [61]. On the contrary, there have been few attempts in utilizing the spray columns for ammonia-based CO_2 capture. Compared with the packed columns, the spray columns have a few advantages, such as low pressure drop, less susceptibility to corrosion, suitability for treating large volumes of flue gas, and greater tolerance to solid precipitation. These features have led to the broad industrial application of spray columns in desulfurization [62]. Kuntz et al. [63] compared the performance of a spray column with a packed column for CO_2 absorption into MEA solution. They found that the spray column was capable of removing CO_2 from gas mixture at a higher rate than that of the packed column. Javed et al. [64] investigated CO_2 absorption into NaOH solution in a high-intensity vortex spray scrubber. The experimental results showed imparting swirl in the gas flow can significantly enhance the overall mass transfer coefficient. Bandyopadhyay et al. [65] used a two-phase critical flow atomizer for CO_2 absorption into dilute NaOH solution, achieving a high CO_2 removal efficiency. Ma et al. [66] investigated various operating conditions on the volumetric overall mass transfer coefficient of ammonia-based CO_2 capture in a spray tower. Very recently, ammonia-based CO_2 capture in a vortex spray scrubber was theoretically and experimentally investigated by Zhao et al. [67]. The studies demonstrated a great potential of using spray columns in CO_2 capture. However, the focus of the studies was mainly concentrated on the influence of operating conditions on CO_2 removal efficiency or mass transfer coefficients. The fundamentals of spray absorption have not been fully understood.

An integrated model combining complex gas-liquid flow and chemical reaction as well as heat transfer is of benefit to comprehensively understand CO_2 absorption process and optimize design of a reactor. In previous studies, Kvamsdal et al. [68] and Lawal et al. [69] employed gPROMS to develop 1-D dynamic models for CO_2 absorption by MEA with the assumption of plug flow regime. Niu et al. [43] used a rate-based model implemented in Aspen Plus to simulate ammonia-based CO_2 capture in a packed column, in which only the axial flow was considered. These 1-D models simplified the complex gas-liquid flow which in fact plays a vital role in the absorption process. In recent studies, much emphasis has been placed on the complex hydrodynamics in absorbers. Niegodajew et al. [70] used the Euler-Euler multiphase models to consider gas-liquid flow in a random packed column. Chu et al. [71] employed the VOF model to consider the gas-liquid flow in a bubble column. For spray columns, Chen et al. [72,73] and Choi [74] theoretically investigated behavior of a single droplet in a spray tower. Zhao et al. [67] investigated the gas flow pattern in a vortex spray column using the RANS model without consideration of reactions. Clearly, there still lacks an integrated model for ammonia-based CO_2 capture in a spray column, limiting the development of ammonia-based CO_2 capture.

In the present work, the principal aim is to establish an integrated model combing the complex gas-liquid flow and the chemistry of the NH_3-CO_2-H_2O system. Both the processes of CO_2 absorption and ammonia slip were taken into consideration. Then, the predicted results were compared with the experimental data from a lab-scale spray column to valid the established model. Moreover, the influence of operating conditions on both CO_2 removal capture and ammonia slip was studied experimentally and theoretically. To reveal the fundamental mechanisms and understand the spray absorption, the validated model was employed to investigate the velocity, temperature and species distributions in the spray column. The understanding will benefit the development of ammonia-based CO_2 capture.

2. Physical models and mathematical formulations

The absorption of CO_2 in a sprayer tower is a typical two-phase flow consisting of continuous flue gas and dispersed liquid droplets. Therefore, the Euler-Lagrange method is adopted due to the advantages of rigorous description of particle-level phenomenon, droplet size distribution, and droplet-wall interaction [75]. The flue gas is treated as a continuum, described by the Eulerian approach, whereas the dispersed droplets are modeled by the Lagrangian approach. Interphase mass and heat transfer is realized via User-defined Functions coupled to the CFD code. Besides, the following assumptions should be made:

(1) The shape of the droplets remains spherical.
(2) Particle-particle interactions in the tower are neglected considering the volume fraction of the droplets is much lower than 10 vol% in the spray reactor except the domain very close to the nozzle.

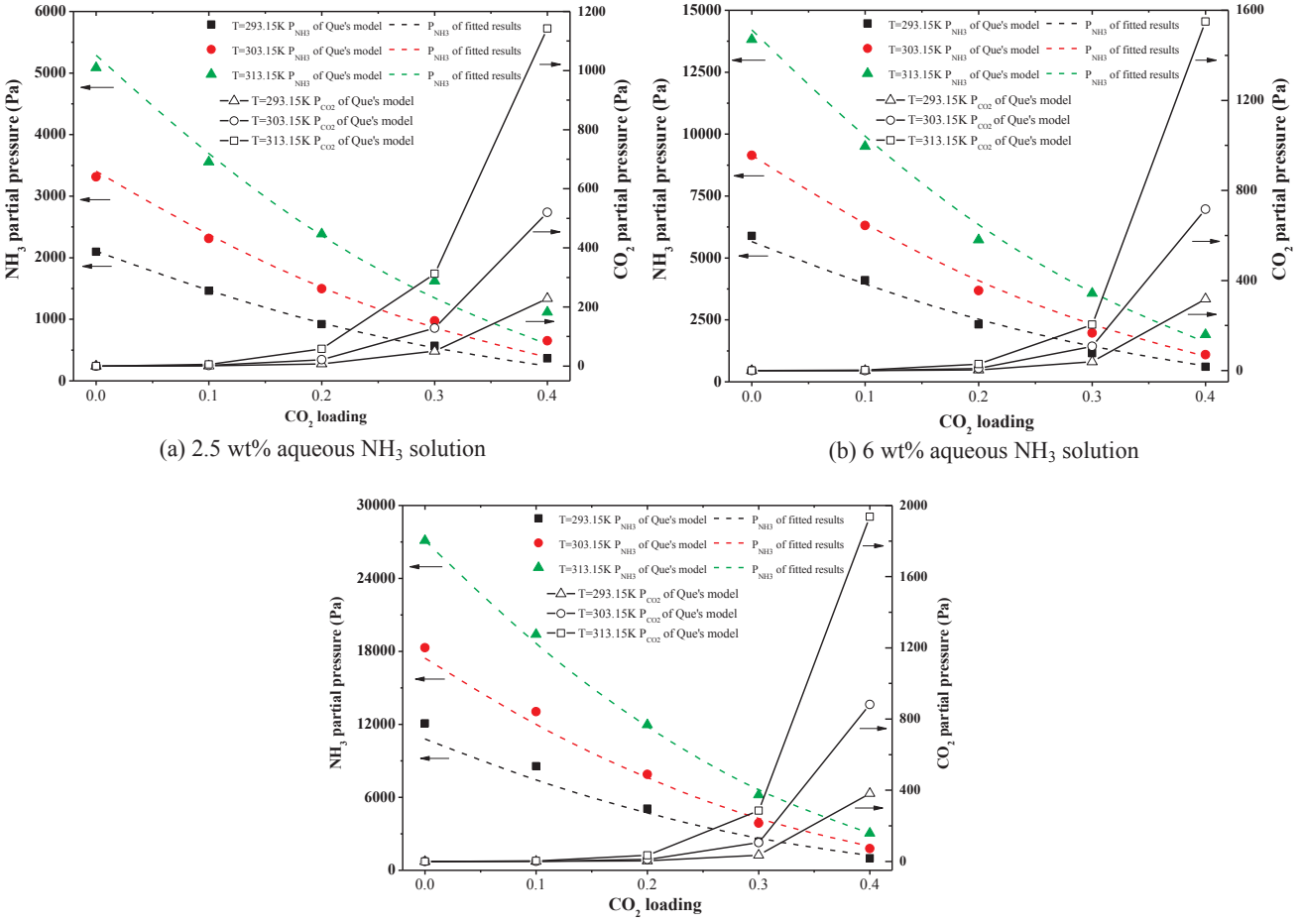
T=293.15K P_NH3 of Que's model
P_NH3 of fitted results
T=303.15K P_NH3 of Que's model
T=313.15K P_NH3 of Que's model
T=293.15K P_CO2 of Que's model
T=303.15K P_CO2 of Que's model
T=313.15K P_CO2 of Que's model
NH3 partial pressure (Pa)
CO2 partial pressure (Pa)
CO2 loading

(a) 2.5 wt% aqueous NH_3 solution

(b) 6 wt% aqueous NH_3 solution

(c) 10 wt% aqueous NH_3 solution

Fig. 1. Comparison of the NH_3 partial pressure predicted from Que's model and that calculated from Eq.14, and the variation of the CO_2 partial pressure predicted by Que's model.

(3) All the reactions are assumed to take place inside the droplets, and the gaseous reactions are neglected. Besides, the precipitation of solid NH_4HCO_3 is neglected considering that the absorption temperature is not lower than 20 °C and the CO_2 loading of ammonia solution is usually lower than 0.5.

2.1. Governing equations

2.1.1. Equations for flue gas

The mass, momentum, energy and species conservation equations of flue gas were expressed in the same formulations of a single phase. The Reynolds-averaged Navier-Stokes equations were employed with the addition of source terms accounting for the interactions with the dispersed droplets [75].

$$\frac{\partial}{\partial t}\rho_g + \nabla \cdot(\rho_g \overrightarrow{u_g}) = S_{mass} \tag{1}$$

$$\frac{\partial}{\partial t}(\rho_g \overrightarrow{u_g}) + \nabla \cdot(\rho_g \overrightarrow{u_g} \times \overrightarrow{u_g}) = -\nabla P_g + \nabla \cdot(\overline{\overline{\tau}} + \tau^R) + \rho_g \overrightarrow{g} + S_{mom} \tag{2}$$

$$\frac{\partial}{\partial t}(\rho_g i) + \nabla \cdot(\rho_g \overrightarrow{u_g} i) = -P_g \nabla \cdot \overrightarrow{u_g} + \nabla \cdot(k_{eff} \nabla T) + S_{en} \tag{3}$$

$$\frac{\partial}{\partial t}(\rho_g w_A) + \nabla \cdot(\rho_g \overrightarrow{u_g} w_A) = \nabla \cdot(\rho_g D_A \nabla w_A) + S_{A,mass} \tag{4}$$

where ρ_g (kg/m^3) is the density of flue gas; $\overrightarrow{u_g}$ (m/s) is the velocity of flue gas; $\overline{\overline{\tau}}$ and τ^R are the shear stress and Reynolds stress tensor, respectively; P_g (Pa) is the pressure of flue gas; T (K) is the temperature of flue gas; i (J/kg) is the internal energy of flue gas; k_{eff} (W/m/K) is the effective thermal conductivity of the flue gas; ω_A is the mass fraction of species A in the flue gas; D_A (m^2/s) is the binary diffusion coefficient of species A in the gas calculated by the correlation proposed by Poling et al. [76]. Based on the Boussinesq hypothesis, the Reynolds stress tensor τ^R is related to the mean velocity gradients. Since the presence of dispersed particles could influence turbulence energy and dissipation rate, it is recommended to add source terms in the equations of k and ε to account for turbulence modulation. However, the experimental results suggest dilute particles have a weak effect on the turbulence modulation [75]. Therefore, the original RNG k-ε model [77] has been adopted to simulate turbulence in the flue gas. The sources terms S_{mass}, S_{mom}, S_{en} and $S_{A,mass}$ represent the mass, momentum, energy and species exchange between the flue gas and the droplets, respectively. All these terms are calculated by volume averaging contributions from all the droplets within the cell.

2.1.2. Equations for droplets

The droplets in the computational domain were modeled by the Lagrangian method. However, it is very computationally expensive to track each individual droplet in computational domain due to the huge number of the droplets. The common practice is to track parcels instead of the droplets. Each parcel is a group of particles assumed to have the same position, velocity, and properties, which also referred to as computational particles [9]. Therefore, the dynamics of droplets in the same parcel can be described by one tracked droplet. According to Marocoo et al. [75,78], the conversation equations for each tracked droplet are expressed as follows:

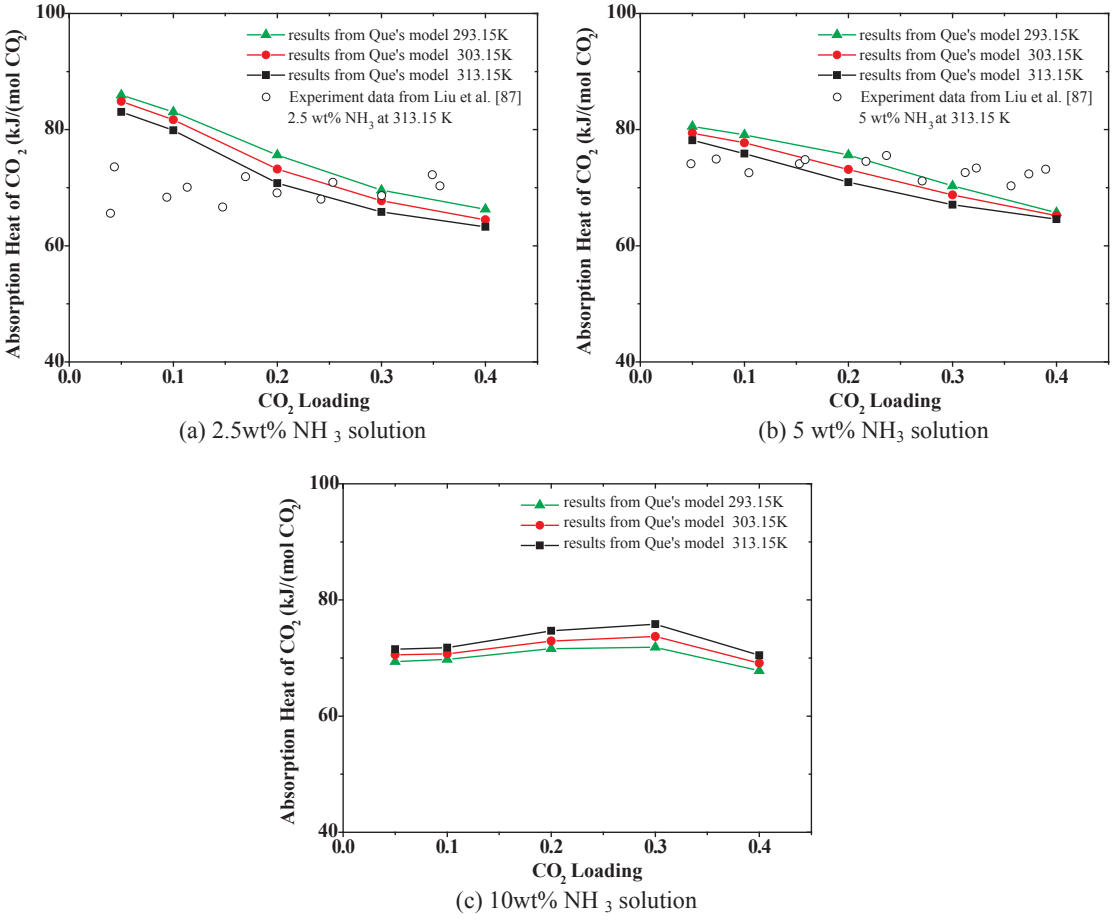
Absorption Heat of CO 2 (kJ/(mol CO2)
CO2 Loading
results from Que's model 293.15K
results from Que's model 303.15K
results from Que's model 313.15K
Experiment data from Liu et al. [87]
2.5 wt% NH3 at 313.15 K
(a) 2.5wt% NH 3 solution
Absorption Heat of CO2 (kJ/(mol CO2)
CO2 Loading
results from Que's model 293.15K
results from Que's model 303.15K
results from Que's model 313.15K
Experiment data from Liu et al. [87]
5 wt% NH3 at 313.15 K
(b) 5 wt% NH3 solution
Absorption Heat of CO2 (kJ/(mol CO2)
CO2 Loading
results from Que's model 293.15K
results from Que's model 303.15K
results from Que's model 313.15K
(c) 10wt% NH 3 solution

Fig. 2. Heat of absorption of CO_2 in ammonia solution calculated from Que's model and that measured in experiments [85].

Table 1
Summary for three proposed mechanisms for carbamte formation.

Mechanisms	Reactions	Formulations
Zwitterion	$NH_3 + CO_2 \underset{k_{-1}}{\overset{k_2}{\rightarrow}} NH_3^+CO_2^-$ $NH_3^+CO_2^- + B \xrightarrow{k_B} NH_2COO^- + BH^+$	$r_{CO_2} = \frac{[CO_2][NH_3]}{1/k_2 + k_{-1}/(k_2 \sum k_B[B])}$ $B = NH_3, H_2O$ $k_2 \sum k_B[B] >> k_{-1}$ $r_{CO_2} = k_2[CO_2][NH_3]$
Termolecular	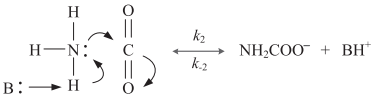	$r_{CO_2} = k_2[CO_2][NH_3]$ $= (k^T_{NH_3}[NH_3] + k^T_{H_2O}[H_2O])[CO_2][NH_3]$
Carbamic acid	$NH_3 + CO_2 \underset{k_{-2}}{\overset{k_2}{\rightarrow}} NH_2COOH$ $NH_2COO^- + H^+ \xrightarrow{k_{eq}} NH_2COOH$	$r_{CO_2} = k_2[CO_2][NH_3]$

$$\frac{dm_d}{dt} = \dot{m}_{NH_3} + \dot{m}_{CO_2} \tag{5}$$

$$m_d \frac{d\overrightarrow{u_d}}{dt} = \frac{1}{2}\rho_g C_D |\overrightarrow{u_g} - \overrightarrow{u_d}|(\overrightarrow{u_g} - \overrightarrow{u_d}) A_d + m_d \vec{g} \tag{6}$$

$$m_d c_{p,d} \frac{dT_d}{dt} = h(T - T_d) A_d + m_{CO_2} \bullet h_R \tag{7}$$

$$m_d \frac{dw_{A,d}}{dt} = \dot{m}_A + M_A \sum_{r=1}^{N} \dot{R}_{A,r} \tag{8}$$

where m_d (kg) is the mass of a droplet; $\dot{m}_A$ (kg/s) is the mass transfer rate of species A, namely, NH_3 and CO_2, and the evaporation of water is neglected due to low absorption temperature; $\overrightarrow{u_d}$ (m/s) is the velocity of a droplet; C_D is the drag coefficient calculated by the Morsi and Alexander correlation [79]; h (W/m^2/K) is the convective heat-transfer coefficient, calculated using the Ranz–Marshall correlation [80]. A_d is the surface of a droplet; h_R (J/kg CO_2) is the heat due to the absorption of 1 kg CO_2, and here the evaporation heat of H_2O and NH_3 is neglected; M_A is the molecular mass of species A; $\dot{R}_{A,r}$ (kmol/s) is the molar rate of production or consumption of species A in the reaction r.

2.1.3. Equations for interphase mass transfer

Both the absorption of CO_2 from the flue gas into the droplets and the escape of NH_3 from the droplets into the flue gas were taken into account in this work. The general interphase mass transfer rate can be expressed as:

$$\dot{m}_A = M_A K_{A,tot} A_d (P_{A,g} - P^{eq}_{A,d}) \tag{9}$$

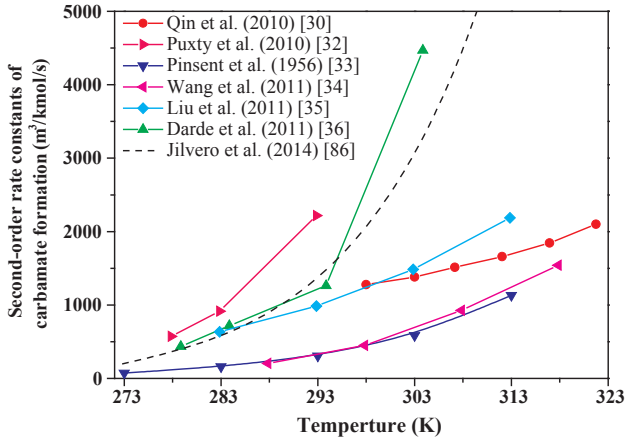

Fig. 3. Comparison of second-order rate constants k_2 as a function of temperature at ammonia concentration of 5 wt%.

where $K_{A,tot}$ (kmol/m^2/Pa/s) is the overall mass transfer coefficient for species A; $P_{A,g}$ is the partial pressure of species A in the flue gas; $P_{A,d}^{eq}$ is the equilibrium pressure corresponding to the concentration of species A in the droplet. The Henry's law is commonly employed to describe the relation between the equilibrium pressure and the concentration in dilute solution. However, considering the non-ideality of the absorbent solution, the real relation of the equilibrium pressure and the concentration can deviate from the Henry's law significantly. Thus, a correlation for the equilibrium pressure is proposed in the following section.

According to the two-film theory, the overall mass transfer resistance $1/K_{A,tot}$ are consisted of liquid-side mass transfer resistance and gas-side mass transfer resistance.

$$\frac{1}{K_{A,tot}} = \frac{1}{k_{A,g}} + \frac{H_A}{Ek^0_{A,aq}} \tag{10}$$

where $k_{A,g}$ (kmol/m^2/Pa/s) is the gas-side mass transfer coefficient; H_A (Pa•m^3/kmol) is the Henry's constant as a function of temperature; E is the mass transfer enhancement factor accounted for the promotion of gas absorption by chemical reactions; $k^0_{A,aq}$ (m/s) is the physical liquid-side mass transfer coefficient.

In the presented model, the Henry's constants of NH_3 and CO_2 are calculated by the correlation proposed by Rumpf and Maurer [81]. The gas-side mass transfer coefficient $k_{A,g}$ is calculated by the modified Ranz–Marshall [82]:

$$Sh = \frac{k_{A,g} D_d RT}{D_A} = 2 + 0.69 \mathrm{Re}_d^{0.5} Sc^{0.33} \tag{11}$$

where D_d is the diameter of a droplet, calculated from the mass and density of a droplet; Re_d is the relative Reynolds number; Sc is the Schmidt number. The physical liquid-side mass transfer coefficient $k^0_{A,aq}$ can be obtained by the correlation proposed by Hsu and Shih [83].

$$k^0_{A,aq} = 0.88\sqrt{fD_{A,aq}} \quad and \quad f = \sqrt{\frac{8\sigma}{3\pi m_d}} \tag{12}$$

where $D_{A,aq}$ (m^2/s) is the diffusion coefficient of species A in aqueous solution; σ (kg/s^2) is the surface tension of the aqueous solution. With respect to the enhancement factor E, it is well known that this factor is dependent on the rates of the chemistry reactions occurring in the liquid phase. Instantaneous, fast, intermediate, and slow regimes are the typical reaction cases [62]. Previous kinetic experiments suggested that the reaction of CO_2 with an ammonia solution should fall under the fast reaction regime [29,31]. Considering the consumption of NH_3 is very little in each calculation step, the reaction occurring in the droplets is approximated by the pseudo-first-order reaction, and assumed to be equal to the Hatta number:

$$E = \frac{\sqrt{k_{app} D_{CO_2,aq}}}{k^0_{A,aq}} \tag{13}$$

where k_{app} (s^{-1}) is the apparent overall kinetic constant.

2.2. Chemistry of the NH_3-CO_2-H_2O system

2.2.1. Thermodynamics of the system

According to the model presented above, the thermodynamics of the NH_3-CO_2-H_2O system are of great importance to the numerical simulation. Que and Chen [28] developed a dedicated thermodynamic model of the NH_3-CO_2-H_2O system with the E-NRTL model. However, Que's model is complex and consisted of several non-linear algebraic equations. To reduce computational cost, several reasonable simplifications of the rigorous thermodynamic model were made in this study. For ammonia partial pressure, a simplified correlation is proposed as Eq. (14), which is regressed from the results of Que's model.

$$p^{eq}_{NH_3} = H_{NH_3}(1-3.4182r + 3.0002r^2)c_{NH_3}\cdot\exp(0.0333c_{NH_3}-0.0123) \tag{14}$$

where r represents the CO_2 loading of solution. The comparison of the

Table 2
Summary for second-order rate constants of carbamate formation.

Sources	Formulations	Conc. range	Temp. range	Mechanism
Qin et al. [30]	$k_2 = k^T_{NH_3}c_{NH_3} + k^T_{H_2O}c_{H_2O}$ $k^T_{NH_3} = 3.996\times10^8\exp(-4455/T)$ $k^T_{H_2O} = 47.314\exp(-306.48/T)$	0.9–5.4 mol/L	25–48 °C	Termolecular
Puxty et al. [32]	$k_2 = 915\exp(-7340(1/T-1/283))$	0.6–6 mol/L	5–20 °C	Carbamic acid
Pinsent et al. [33]	$k_2 = 1.35\times10^{11}\exp(-5844/T)$	Dilute solution	0–40 °C	Carbamic acid
Wang et al. [34]	$k_2 = 9.17\times10^{10}\exp(-5691/T)$ $k_{-2} = 5.7\times10^{13}\exp(-8182/T)$	2–16 mmol/L	15–40 °C	Carbamic acid
Liu et al. [35]	$k_2 = k^T_{NH_3}c_{NH_3} + k^T_{H_2O}c_{H_2O}$ $k^T_{NH_3} = 1.185\times10^7\exp(-3268/T)$ $k^T_{H_2O} = 8.533\times10^6\exp(-4017/T)$	0.53–4 mol/L	10–40 °C	Termolecular
Darde et al. [36]	$k_2 = 4900\exp(-14000(1/T-1/283))$ $\frac{k_2k_{NH_3}}{k_{-1}} = 210\exp(-2200(1/T-1/283))$ $\frac{k_2k_{H_2O}}{k_{-1}} = 0.71\exp(-18000(1/T-1/283))$	1-10 wt% (0.59–5.65 mol/L)	6–31 °C	Zwitterion
Jilvero et al. [84]	$k_2 = 6.51\times10^{13}\exp(-7235/T)$ $k_{-2} = 1.27\times10^{22}\exp(-9659/T)$	—	—	Carbamic acid

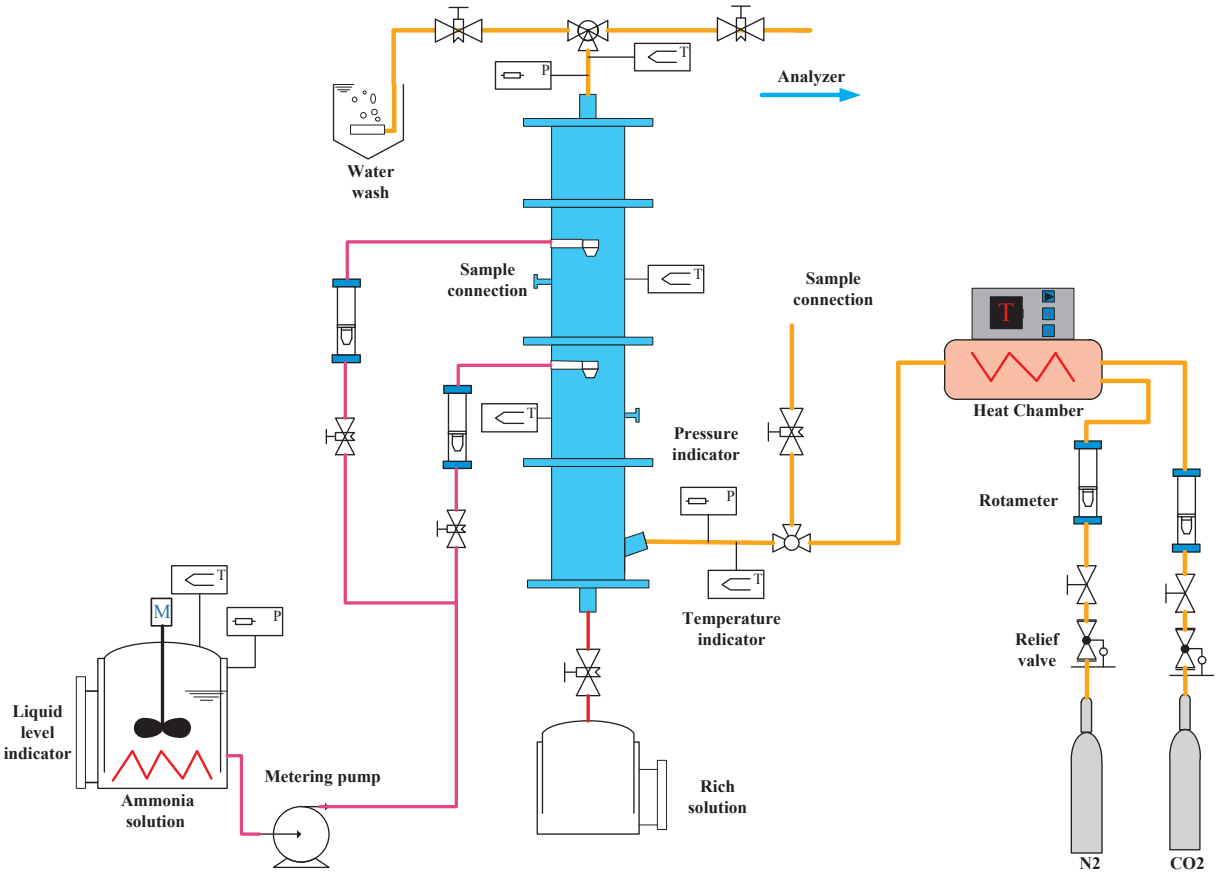

Fig. 4. The schematic diagram of experimental spray system for CO_2 absorption.

Table 3
A variety of operating conditions of experiments (CO_2 concentration in the fresh flue gas was maintained at 15 vol% in all experiments).

Case NO.	Aqueous NH_3 Concentration	Solution temperature	Solution flow rate	Gas flow rate	Inlet gas temperature
Influence of gas flow rate					
Case 1	5 wt%	20 °C	2 L/min	6 m^3/h	20 °C
Case 2	5 wt%	20 °C	2 L/min	8 m^3/h	20 °C
Case 3	5 wt%	20 °C	2 L/min	10 m^3/h	20 °C
Case 4	5 wt%	20 °C	2 L/min	12 m^3/h	20 °C
Influence of NH_3 concentration of the solution					
Case 5	2.5 wt%	20 °C	2 L/min	6 m^3/h	20 °C
Case 6	7.5 wt%	20 °C	2 L/min	6 m^3/h	20 °C
Case 7	10 wt%	20 °C	2 L/min	6 m^3/h	20 °C
Influence of the temperature of the solution					
Case 8	5 wt%	30 °C	2 L/min	6 m^3/h	20 °C
Case 9	5 wt%	40 °C	2 L/min	6 m^3/h	20 °C
Case 10	5 wt%	50 °C	2 L/min	6 m^3/h	20 °C
Influence of the flow rate of the solution					
Case 11	5 wt%	20 °C	1.5 L/min	6 m^3/h	20 °C
Case 12	5 wt%	20 °C	2.5 L/min	6 m^3/h	20 °C
Case 13	5 wt%	20 °C	3 L/min	6 m^3/h	20 °C

NH_3 partial pressure predicted by Que's model and that calculated from Eq. (14) is illustrated in Fig. 1. In addition, the variation of the CO_2 partial pressure predicted by Que's model is also shown in Fig. 1. It can be seen the ammonia partial pressure calculated by Eq. (14) presents a reasonable agreement with that predicted by Que's model. The CO_2 partial pressure approaches to 0 Pa at low CO_2 loading (< 0.2). When the CO_2 loading increases over 0.3, the CO_2 partial pressure grows exponentially. Therefore, Jilvero et al. [84] suggested that the CO_2 loading of rich solution should be operated below 0.3. In this paper, the equilibrium CO_2 partial pressure was assumed to be equal to 0 Pa since fresh ammonia solution was used as absorbent.

For reaction heat, the global reactions R1-R3 and corresponding heat are thoroughly discussed by Jilvero et al. [84] and Liu et al. [85]

$$CO_2 + NH_3 + H_2O \leftrightarrow NH_4^+ + HCO_3^- \quad \Delta H = 64.26\ \text{kJ/mol CO}_2 \tag{R1}$$

$$CO_2 + 2NH_3 \leftrightarrow NH_4^+ + NH_2COO^- \quad \Delta H = 72.32\ \text{kJ/mol CO}_2 \tag{R2}$$

$$CO_2 + 2NH_3 + H_2O \leftrightarrow 2NH_4^+ + CO_3^{2-} \quad \Delta H = 101.22\ \text{kJ/mol CO}_2 \tag{R3}$$

Moreover, Fig. 2 shows the heat of absorption of CO_2 in ammonia solution predicted by Que's model and that measured in experiments [85]. It can be seen that the predicted and experimental results indicate the heat of absorption does not change significantly with temperature and CO_2 loading as well as ammonia concentration. We also note that the heat of absorption of CO_2 in ammonia solution is comparable with the heat released by carbamate formation (Eq. (R2)). This is due to the fact that the formation of carbamate is the predominant process at low CO_2 loading (< 0.5) [86,87]. Therefore, it is reasonable to make the assumption that the heat of absorption of CO_2 in our model is equal to the reaction heat of cabarmate formation.

2.2.2. Kinetics of the NH_3-CO_2-H_2O system

The carbamate pathway Eq. (R2) has been considered as the main reaction for absorption at low CO_2 loading. However, detailed reaction mechanism is still in a controversy. Table 1 summarizes the three mechanisms proposed for the formation of carbamate, including the zwitterion mechanism, the termolecular mechanism, and the carbamic acid mechanism [30,34]. Fig. 3 shows the second-order reaction rate constants of carbamate formation at ammonia concentration of 5 wt%.

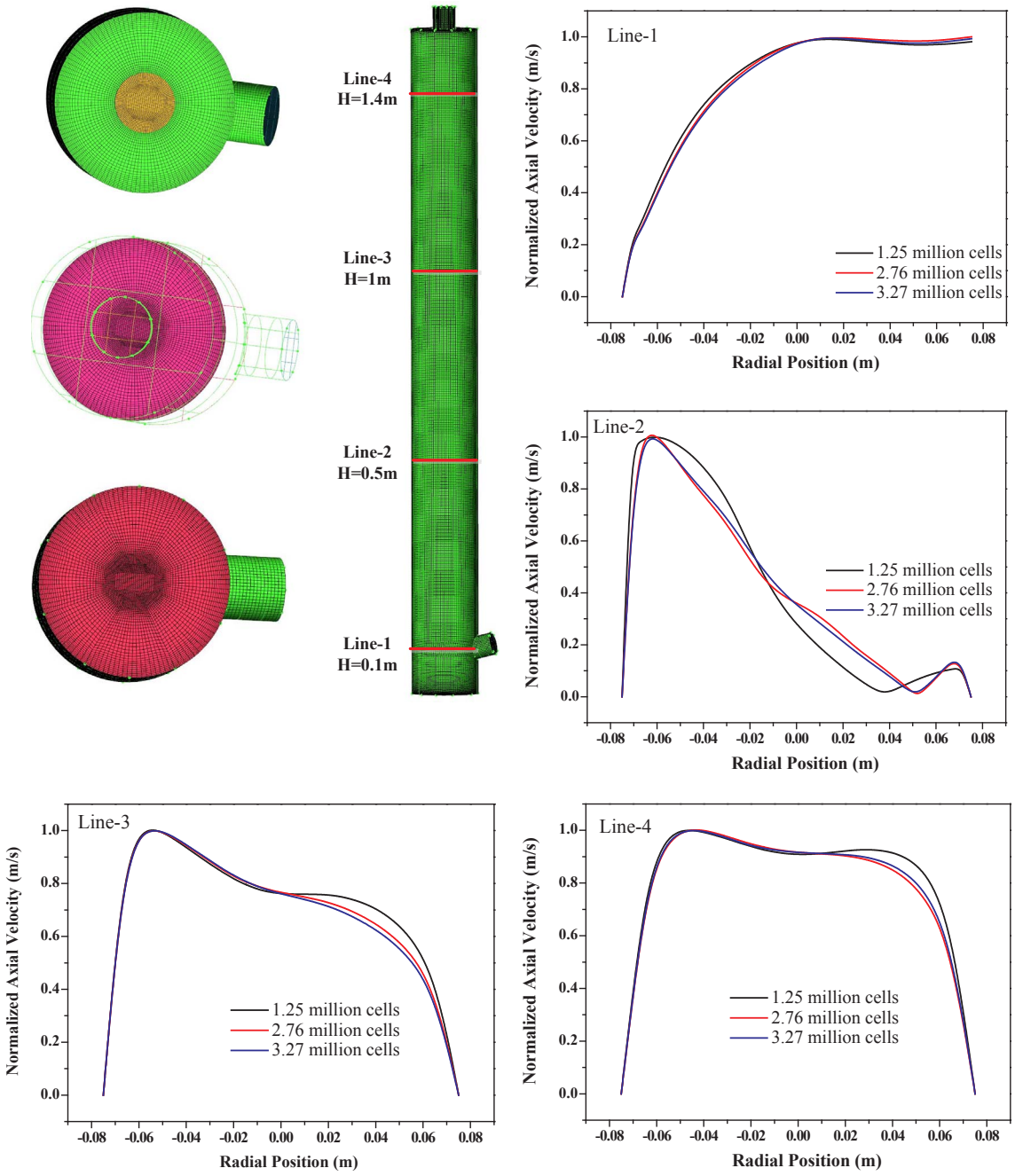

Fig. 5. Computional mesh and mesh independence test

The formulations and experimental conditions are listed in Table 2. A substantial divergence of the second-order reaction rate constants can be seen in Fig. 3. Wang's rate constant agrees well with Pinsent's rate constant, whereas Jilvero's rate constant (dash line, calculated from logarithmic mean of Pinsent's rate constant and Puxty's rate constant) is comparable with Darde's rate constant. It is also seen that Liu's rate constant and Qin's rate constant are in the medium. Examining the experimental concentration in Table 2, it is interesting to note that both Wang's and Pinsent's rate constants, the slowest rates, are measured at low ammonia concentration, while Puxty's rate constant, the fastest rate, is measured at high ammonia concentration. This suggests that the second-order rate constant increases with ammonia concentration. This viewpoint was also supported by Qin et al. [30] from a statistical perspective. They found the fitting results from the termolecular mechanism were more robust than those from the zwitterion mechanism. In this paper, the second-order rate constants from Liu et al., Pinsent et al., and Jilvero et al. were tested by comparison between simulation and experimental data. For the reverse reaction of carbamate formation, only Wang et al. directly reported their fitting results from experimental data, which is employed in our model.

3. Experiments

Fig. 4 illustrates the schematic diagram of the experimental spray system for CO_2 absorption. The simulated flue gas in experiments was prepared by mixing CO_2 and N_2 from gas cylinders, and then heated to the desired temperature in a heat chamber. CO_2 concentration in the fresh flue gas was measured from the sample connection at inlet and maintained at 15 vol% in all experiments. After that, the flue gas was fed into the bottom of the absorption tower. The absorption tower was

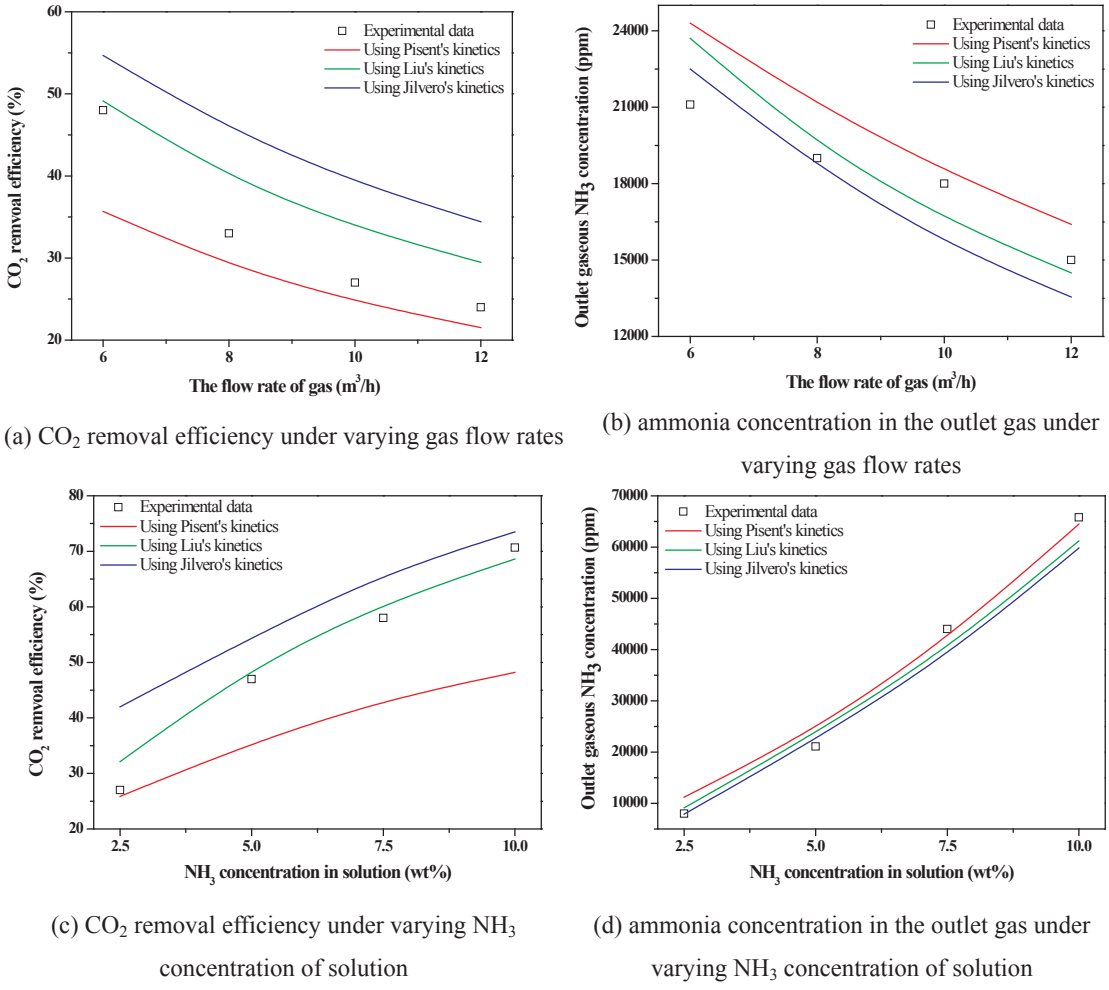

(a) CO_2 removal efficiency under varying gas flow rates

(b) ammonia concentration in the outlet gas under varying gas flow rates

(c) CO_2 removal efficiency under varying NH_3 concentration of solution

(d) ammonia concentration in the outlet gas under varying NH_3 concentration of solution

Fig. 6. Comparisons of predicted and experimental results under various operating conditions.

made of organic glass with a height of 1.5 m and an inner diameter of 0.15 m. Two solid-cone pressure swirl nozzles (JJXP-030, H.lkeuchi & Co.,Ltd) were installed at 1.0 m and 1.2 m to the bottom of the tower, respectively. However, only the nozzle installed at 1.2 m was utilized in the present work. Aqueous ammonia solution was stored in a tank equipped with a stirrer and electrically heated wires. During absorption, the solution was pumped through the nozzles to form droplets, which counter-current contacted with upward simulated flue gas. Both the gas and solution flow rates were controlled by a series of rotameters. Moreover, two sample taps and two temperature indicators were arranged along the tower, to monitor the variations of temperature and gas component.

In the present study, seventeen different cases were investigated. The experimental conditions of each case were listed in Table 3. As can be seen in Table 3, both gas and solution flow rates, the NH_3 concentration of solution, and both gas and solution temperature were varied. CO_2 and NH_3 concentrations in flue gas as well as flue gas temperature at outlet and along the tower were measured. In all experiments, the gaseous concentrations of CO_2 and NH_3 were measured by a dual-channel gas analyzer (SIEMENS, Ultramat 6E). The detection range of the analyzer is 0–20 vol% for CO_2 and 0–30,000 ppm for NH_3, respectively, with the accuracy of ± 1% F.S. With respect to gaseous ammonia concentration over 30,000 ppm, a gas stream of N_2 was introduced to dilute the ammonia concentration to the detection range.

4. Numerical simulation

Due to the simple geometry, uniform grids were generated using multi-block structured method with hexahedral mesh. The mesh independence was carefully tested using three mesh systems as shown in Fig. 5. The results from the mesh system using 2.76 million cells and 3.27 million cells were comparable, while a remarkable difference was observed in the results from the mesh system using 1.25 million cells. Therefore, the mesh systems with 2.76 million cells were adopted considering a promising comprise between accuracy and computational efficiency. The nozzle has been treated as injection points instead of geometric modeling. The distribution of droplet size was represented by the Rosin-Rammler correlation according to the data from the company. For the pressure-velocity coupling, the predictor-corrector SIMPLE algorithm was used. Spatial derivatives were discretized by the second-upwind scheme, while the gradients were computed with the least squares cell based method. For droplet-wall interaction, wall-film model was employed to account for the complex physical phenomenon based on the impact energy [88]. For the benefit of convergence, the under-relaxation coefficients of the energy and discrete phase source were initially set at 0.7 and 0.2, respectively.

5. Results and discussion

In this section, model validation was performed and discussed firstly. The results from the presented model integrating three different kinetics, respectively, i.e., Pinsent's kinetics, Liu's kinetics and Jilvero's kinetics were compared with the experimental results obtained under various operating conditions. In addition, the validated model was used to investigate the influence of varying conditions on the distribution of velocity, gaseous CO_2 and NH_3, and temperature, to reveal the

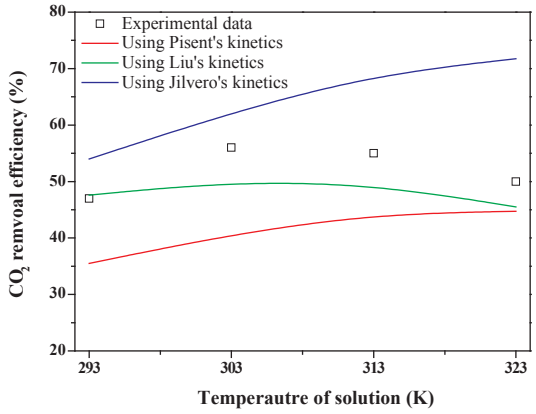

(e) CO_2 removal efficiency under varying temperature of solution

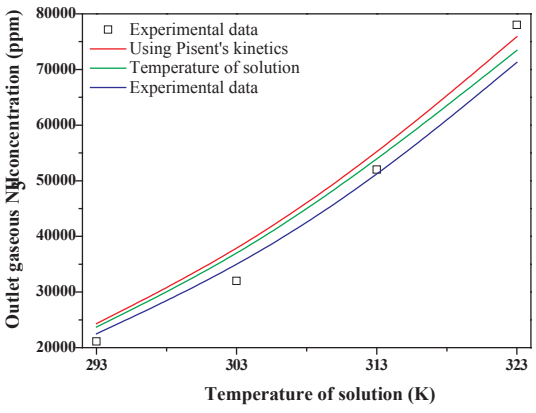

(f) ammonia concentration in the outlet gas under varying temperature of solution

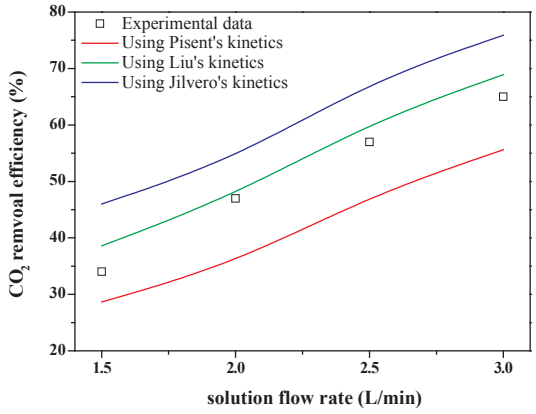

(h) CO_2 removal efficiency under varying solution flow rate

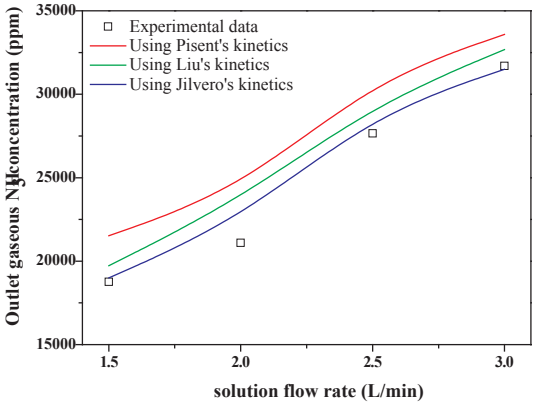

(i) ammonia concentration in the outlet gas under varying solution flow rate

Fig. 6. (*continued*)

fundamentals of spraying absorption.

5.1. Model validation

To valid the models using different kinetics, Fig. 6 compares the experimental CO_2 removal efficiency and NH_3 concentration in the outlet gas with the corresponding predicted results under various operating conditions. Fig. 6a and Fig. 6b present the variations of experimental and predicted results as the gas flow rate increases from 6 m^3/h to 12 m^3/h. The CO_2 removal efficiency drops down from 48.2% to 23.7% in experiments, which lies between the predictions obtained using Liu's kinetics and Pinsent's kinetics. However, it is worth noting that the prediction obtained using Jilvero's kinetics overestimates the efficiency, suggesting that the Jilvero's reaction rate is too fast comparing to the experiment. Besides, although predicted efficiency using Pinsent's kinetics is much lower than the experimental one at the gas flow rate of 6 m^3/h, the agreement at high gas flow rate is good. For the NH_3 concentration in the outlet gas, the experimental ones decrease from 21178 ppm to 15146 ppm. All the predicted results show the consistent decreasing trend. This is because of the utilization of the same NH_3 evaporation model. In addition, the kinetics only has minor influence on the NH_3 escape. Due to the lowest reaction rate, the NH_3 concentration in the outlet gas predicted using Pinsent's kinetics is always the highest among the three models.

Fig. 6c and Fig. 6d compare the variations of the experimental and predicted results with the increase of NH_3 concentration of solution. For CO_2 removal efficiency, although all the predicted efficiencies increase with the NH_3 concentration of solution, the results predicted using Liu's kinetics present a better consistency with the experimental results. This might be due to the consideration of the NH_3 concentration effect on the second-order rate constant in Liu's kinetics. For the ammonia concentration in the outlet gas, again results predicted from all three kinetics are similar to the experimental data.

The comparison of the experimental and predicted results under various solution temperatures is shown in Fig. 6e and Fig. 6 f. As liquid temperature increases from 293 K to 303 K, the CO_2 removal efficiency in experiments firstly increases from 48.2% to 56.0%. However, the efficiency starts to decline when the liquid temperature is higher than 303 K. This alternation is also observed in Zeng's studies on a spray reactor [89] and Niu's studies on a packed reactor [43]. In their studies, the highest CO_2 removal efficiency occured at 306 K and 313 K, respectively. This feature is only predicted using Liu's kinetics. For Jilvero's kinetics, the growth of their reaction rate with temperature is too fast as can be seen in Fig. 3. With respect to Pinsent's kinetics, due to the low reaction rate, the predicted efficiency grows slowly with the solution temperature. For ammonia concentration in the outlet gas, both the experimental and predicted results increase rapidly with the increase of solution temperature.

Fig. 6h and Fig. 6i demonstrate the variations of the experimental and predicted results as NH_3 solution flow rate increases. The increasing solution flow rate can increase the number of droplets, and reduce the average diameter of droplets. All the predicted efficiency presents the same varying trend with the experimental efficiencies. However, the efficiency predicted using Liu's kinetics is better in

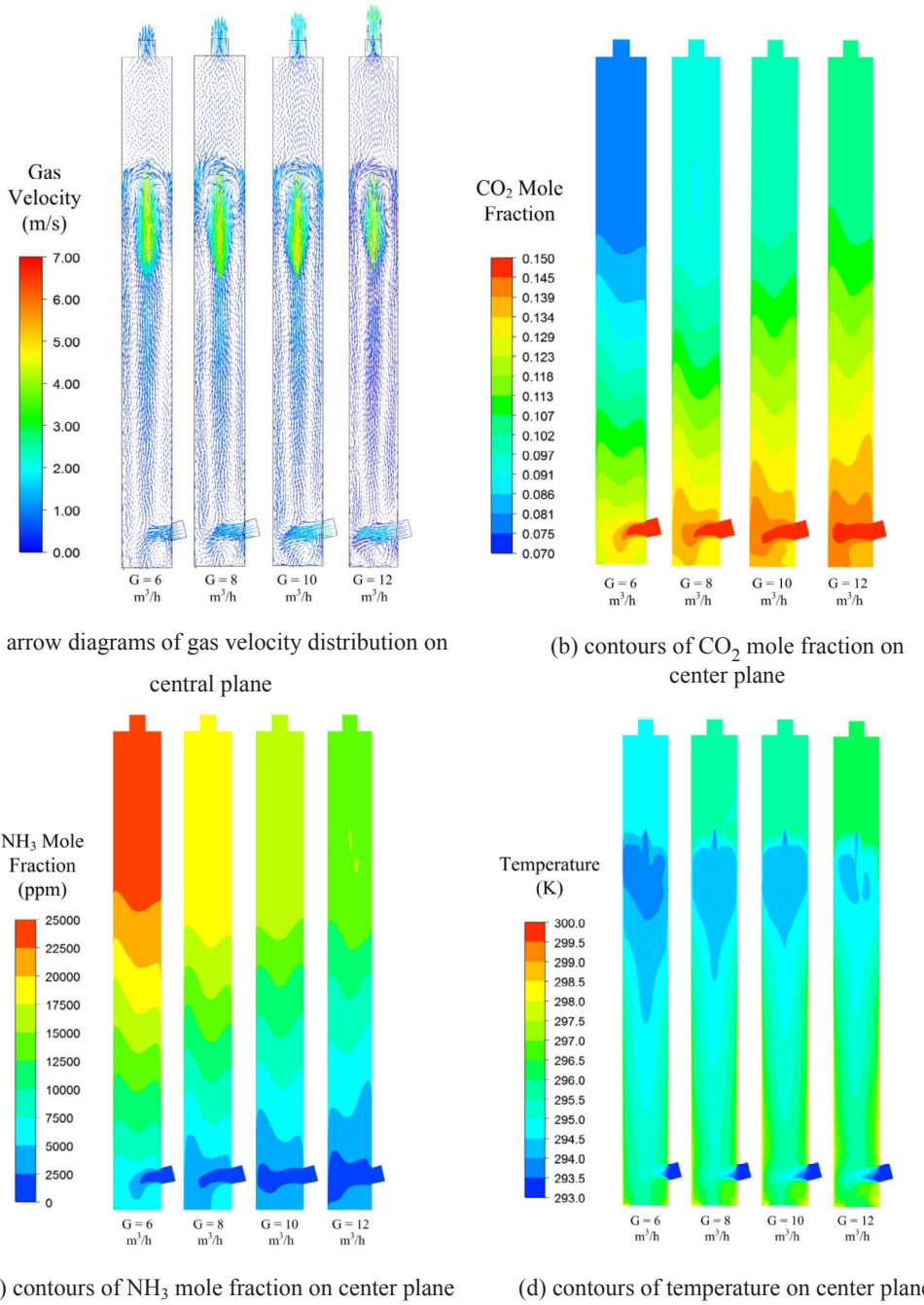

(a) arrow diagrams of gas velocity distribution on central plane

(b) contours of CO_2 mole fraction on center plane

(c) contours of NH_3 mole fraction on center plane

(d) contours of temperature on center plane

Fig. 7. Variations of distribution of gaseous velocity, CO_2 and NH_3 mole fraction, and temperature with the increase of gas flow rate.

accordance with the experimental data. For the ammonia concentration in the outlet gas, an acceptable accuracy between experimental and predicted results is achieved. According to the discussion above, the model using Liu's kinetics shows a reasonable agreement with the experiments. Therefore, this model is employed to investigate detailed spraying characteristics in the following sections.

5.2. Effect of gas flow rate

The influence of gas flow rate on the distribution of gaseous velocity, CO_2 and NH_3 concentration, and temperature is illustrated in Fig. 7. The gaseous velocity profile is firstly investigated in Fig. 7a. It is seen in the arrow diagrams that the hydrodynamics in the spray reactor is complex and several vortexes are observed. Due to the jet flow effect of droplets, portions of the upward flue gas nearby the nozzle turns to flow downwards with the droplets, until it reaches the inlet of the reactor. At the inlet, the downward flue gas mixes with the inlet fresh flue gas and turns to flow upwards along the wall. This back-mixing phenomenon can reduce the driving force for CO_2 absorption. Examining the Fig. 7a from left to right, the increasing gas flow rate has limited influence on the gaseous velocity distribution, suggesting the spray effect is dominant in our experimental system. Accordingly, due to the hydrodynamics effects, the gaseous concentrations of CO_2 and NH_3 as well as the temperature distribute unevenly, particularly in the lower part of the reactor. In Fig. 7b and Fig. 7c, the downward flue gas has a lower CO_2 concentration and a higher NH_3 concentration than that of the upward flue gas along the wall, indicating that hydrodynamics has a remarkable influence on the CO_2 and NH_3 distribution. In the region near the nozzle, it is noted the CO_2 and NH_3 concentration tends to be evenly distributed. This is mainly due to the strong mixing effect of spray. For the temperature profile in Fig. 7d, the injected droplets initially form a region of low temperature near the nozzle.

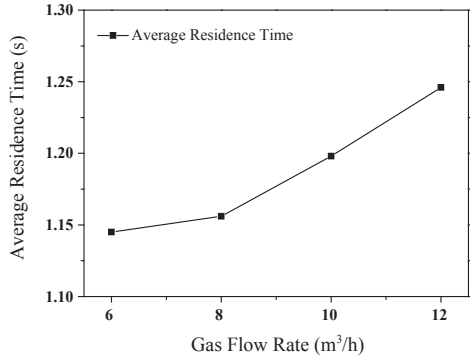

(a) Influence of gas flow rate on average residence time

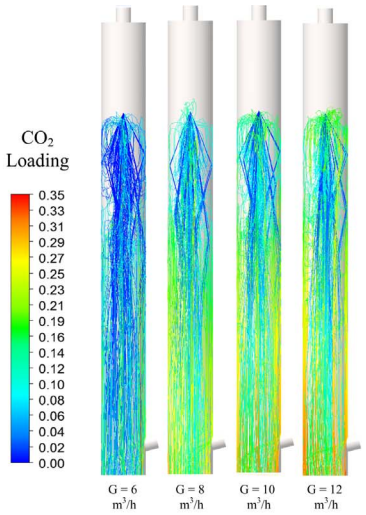

(b) droplets pathlines colored by CO_2 loading

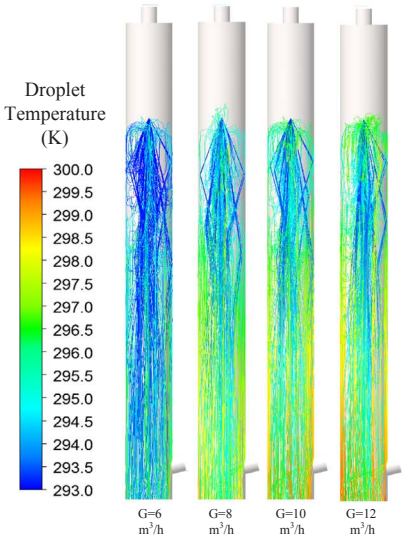

(c) droplets pathlines colored by temperature

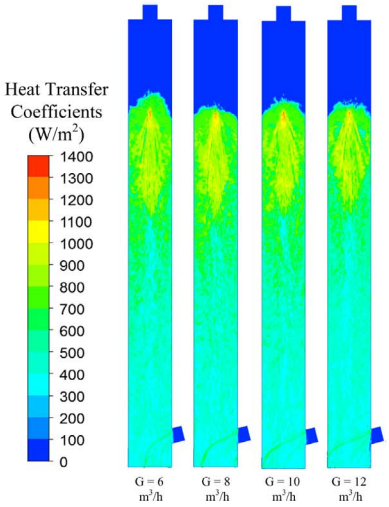

(d) center plane contours for heat transfer coefficient

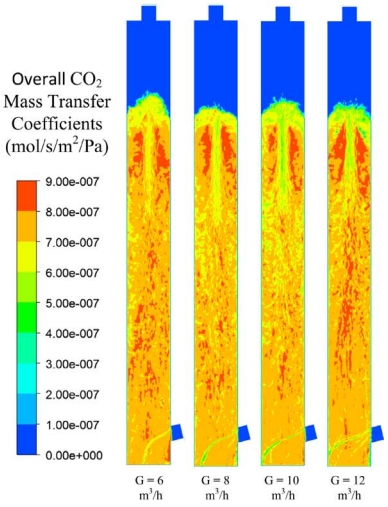

(e) center plane contours for overall CO_2 mass transfer coefficients

Fig. 8. the influence of gas flow rate on spray absorption

Due to exothermic reaction of CO_2 and NH_3, both droplets and gas are warmed up. As gas flow rate increases, it is interestingly noted that the outlet gas temperature increases and evidently the region of low temperature also is reduced.

For better understanding the phenomena observed above, we further investigated the variations of droplet residence time, droplet temperature, CO_2 loading, and interphase mass and heat transfer coefficients in Fig. 8. As can be seen in Fig. 8a, the average residence time of droplets is prolonged from 1.145 s to 1.246 s with the increasing gas flow rate. The prolonged residence time can lead to an increase in both droplet temperature and CO_2 loading. For a clear observation, pathlines of two hundred sampled droplets colored by CO_2 loading and temperature are presented in Fig. 8b and Fig. 8c, respectively. As expected, both the droplet temperature and CO_2 loading are increased. Besides the prolonged residence time, increased gaseous CO_2 concentration (as can be seen in Fig. 7b) improves the driving force for CO_2 absorption, which also leads to an increase in droplet temperature and the CO_2 loading. This can explain the increasing outlet gas temperature observed above. Fig. 8d and Fig. 8e illustrate the variations of interphase heat and overall CO_2 mass transfer coefficients with the gas flow rate. As can be seen, both the coefficients vary slightly with the gas flow rate, which agrees with the conclusion that the liquid-side resistance is dominated for ammonia-based CO_2 absorption.

5.3. *Effect of NH_3 concentration of solution*

Fig. 9 illustrates the influence of the NH_3 concentration of solution on spray absorption. According to the two film theory and Liu's kinetic model, increasing NH_3 concentration of the solution has a promoted effect on CO_2 absorption. Examining Fig. 9a from left to right, the colors of the contours change from cyan for 2.5 wt% ammonia solution to red for 10 wt% ammonia solution, indicating the overall CO_2 mass transfer coefficient increases significantly with the NH_3 concentration of solution. As a consequence, the gaseous CO_2 mole fraction is evidently reduced with the NH_3 concentration of solution in Fig. 9b. Due to the heat of absorption of CO_2, the temperature in the reactor also increases with the NH_3 concentration of solution. The low temperature region around the nozzle is also clearly reduced. However, both the increase on NH_3 concentration of solution and temperature has a promoted effect on ammonia escape. As can been seen in Fig. 9d, the gaseous NH_3 concentration increases significantly when NH_3 concentration of the solution increases from 2.5 wt% to 10 wt%.

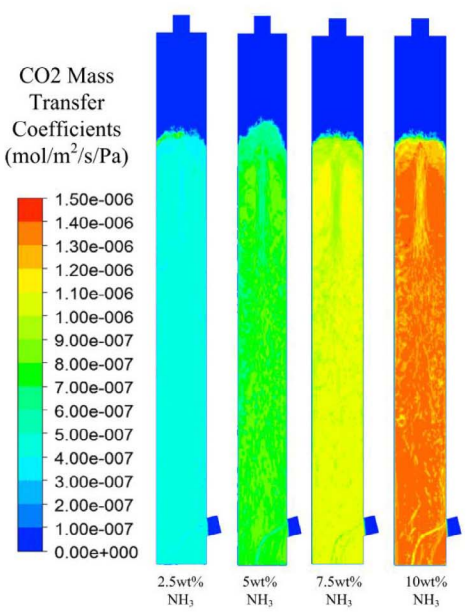

(a) Center plane contours for CO_2 mass transfer coefficient

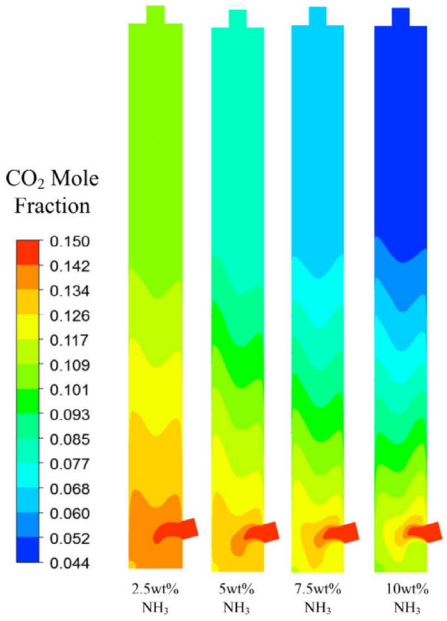

(b) Center plane contours for gaseous CO_2 mass mole fraction

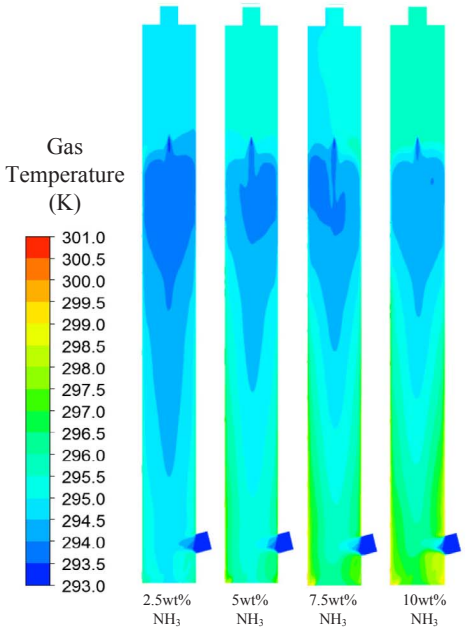

(c) Center plane contours for gas temperature

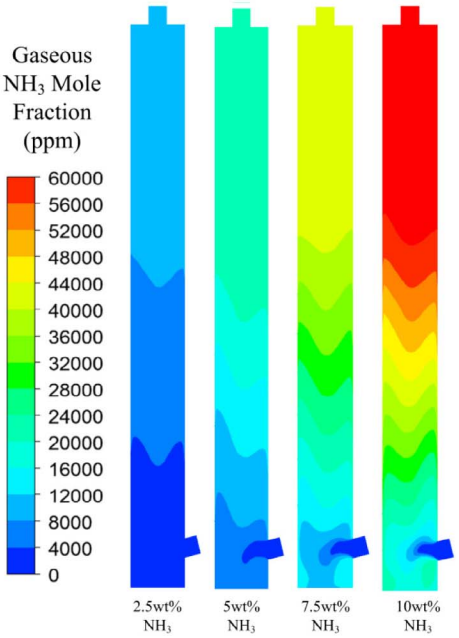

(d) Center plane contours for gaseous NH_3 mole fraction

Fig. 9. The influence of the NH_3 concentration of solution of spray absorption.

5.4. *Effect of solution temperature*

Fig. 10 illustrates the effect of solution temperature on spray absorption. It can be seen in Fig. 10a from left to right, the colors of the contours vary from nearly all blue (representing the solution temperature of 293 K) to red (representing the solution temperature of 323 K). Besides, due to the exothermic reaction, the outlet gas temperature is always slightly higher than the solution temperature. Due to the utilization of wall-film model considering for the wall effect, the highest gas temperature is always observed nearby the wall at the bottom. The increasing solution temperature has complex effects on CO_2 mass transfer coefficients. On the one hand, the reaction rate of NH_3 with CO_2 increases with the temperature, improving the mass transfer enhancement factor *E*. On the other hand, the Henry's constant for CO_2 also increases with liquid temperature, leading to an increase in liquid mass transfer resistance. As a combined result, the overall CO_2 mass transfer coefficient gradually increases with the solution temperature in Fig. 10b. However, in Fig. 10c, it is observed that the outlet gaseous CO_2 mole fraction firstly slightly decreases as the solution temperature increases from 293 K to 303 K, and then it increases slightly as the liquid temperature increases from 313 K to 323 K. The former decrease of the gaseous CO_2 mole fraction at low temperature range can be explained by the improvements of the overall CO_2 mass transfer coefficients. For the latter increase at high temperature range, it can be

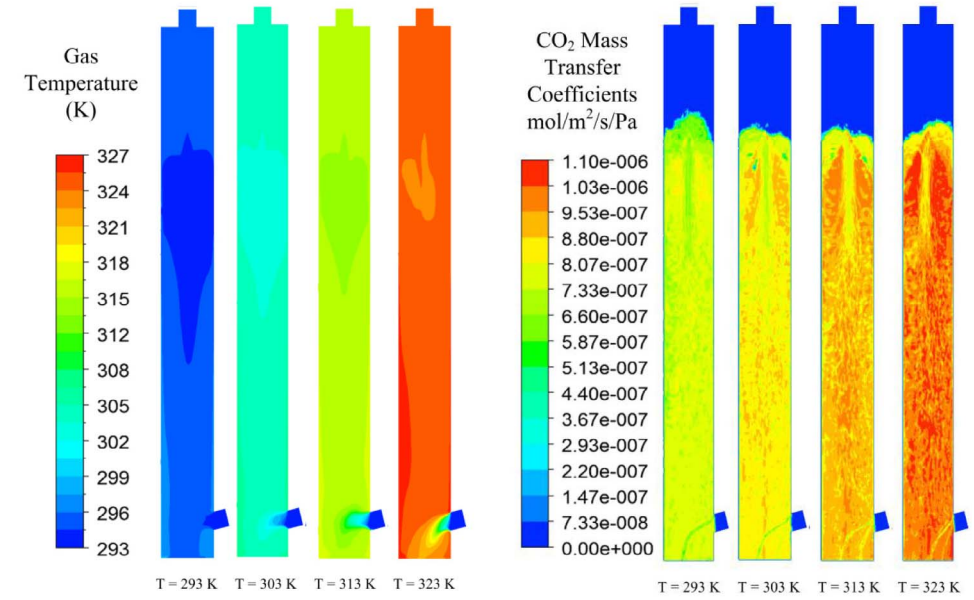

(a) Center plane contours for gas temperature

(b) Center plane contours for CO_2 mass transfer coefficients

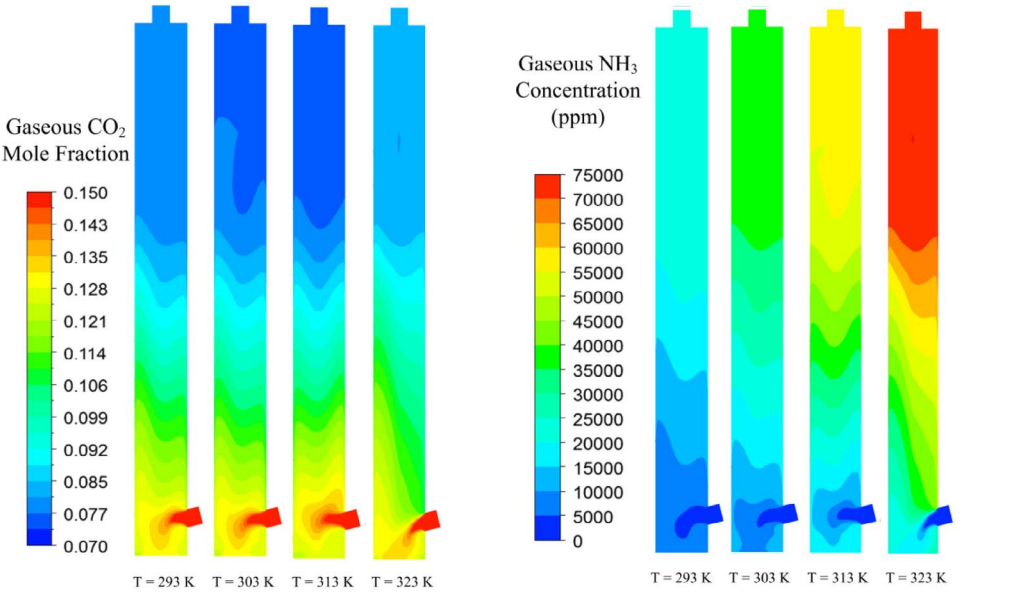

(c) Center plane contours for gaseous CO_2 mole fraction

(d) Center plane contours for gaseous NH_3 mole fraction

Fig. 10. The influence of solution temperature on spray absorption.

attributed to the promotion of the reverse reaction rate and the increasing concentration of product in the solution with the increase of solution temperature. For ammonia escape, it is seen in Fig. 10d that the ammonia concentration in flue gas increases significantly with the solution temperature.

5.5. *Effect of solution flow rate*

Solution flow rate can has a vital effect on the spray, involving initial velocity of droplets, number of droplets, and diameters of droplets. Fig. 11 illustrates the variations of gaseous velocity, CO_2 and NH_3 concentration, temperature and overall CO_2 mass transfer coefficients with solution flow rate. As can be seen in Fig. 11a, except that the gaseous velocity near the nozzle increases with the solution flow rate, there are limited variations in gaseous flow velocity under different solution flow rate conditions. Examining the Fig. 11b from left to right, the gaseous CO_2 mole fraction gradually decreases with the solution flow rate. However, the overall CO_2 mass transfer coefficients illustrated in Fig. 11e varies slightly with the solution rate. This suggests that the decrease in gaseous CO_2 mole fraction is due to the increase of interphase area. The increased interphase area also has a negative effect on ammonia escape. As can be seen in Fig. 11c, the gaseous ammonia mole fraction increases gradually with the solution rate. For the variations of temperature, although the outlet gas temperature remains the same, the region of low temperature nearby the nozzle is extended with the increasing solution flow rate.

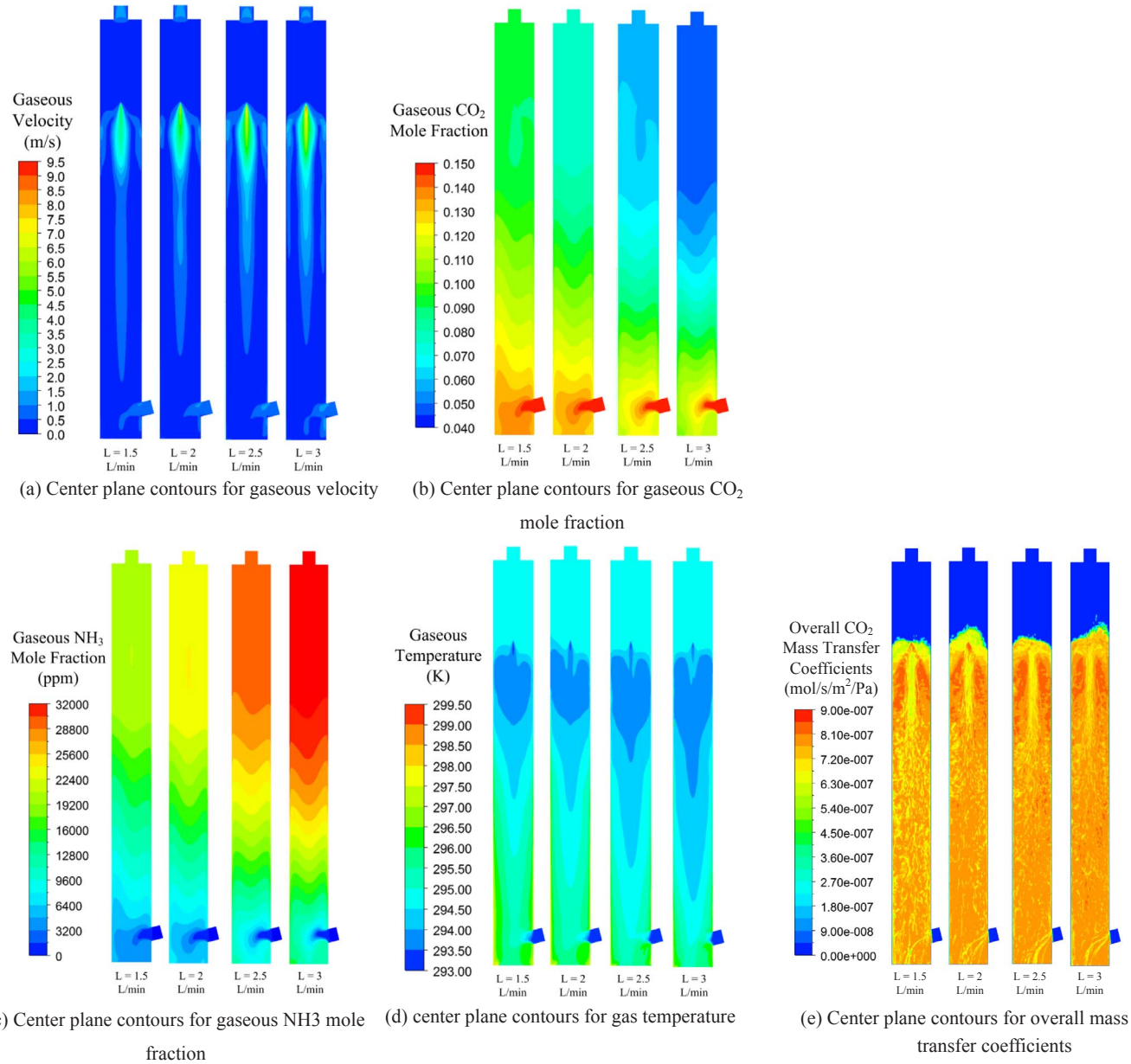

(a) Center plane contours for gaseous velocity

(b) Center plane contours for gaseous CO_2 mole fraction

(c) Center plane contours for gaseous NH3 mole fraction

(d) center plane contours for gas temperature

(e) Center plane contours for overall mass transfer coefficients

Fig. 11. The influence of the solution rate on spray absorption.

6. Conclusions

In order to optimize the design and operation of ammonia-based CO_2 capture process, a three-dimensional numerical model integrating the complex gas-liquid hydrodynamics and the chemistry of the NH_3-CO_2-H_2O system has been developed. A laboratory scale spray absorption system was established and run under various operating conditions to validate the model developed. It was found that the simulated results using Liu's kinetics present a better agreement with the experimental results, especially when NH_3 concentration and temperature of the solution vary.

Using the validated model, the impact of operating parameters on the distribution of gaseous velocity, temperature, gaseous CO_2 and NH_3 concentration in the reactor has been studied to reveal the fundamentals of spray absorption. It has been found that the gas temperature profile as well as gaseous CO_2 and NH_3 concentration profile depends on the velocity field, indicating the hydrodynamics should be considered when optimizing the design of reactor. It has also been found that the average residence time of droplets is prolonged with the increase of gas flow rate, resulting in the increase in the gas temperature, while the increasing NH_3 concentration of the solution could significantly improve the overall CO_2 mass transfer coefficient. The overall CO_2 mass transfer coefficient together with the CO_2 removal efficiency was found to grow with the increase of the liquid temperature in low temperature range. However, the reverse reaction rate would increase with the increase of the liquid temperature, resulting in the decrease of CO_2 removal efficiency at high temperature range. In addition, the increase of liquid flow rate would mainly increase the interphase area and promote both CO_2 absorption and NH_3 escape.

In order to optimize the design of reactor, further numerical investigation of the influence of various design parameters, e.g., absorber structure and arrangements of nozzles, on spray absorption is being undertaken by authors at the moment and the results will be reported in near future.

Acknowledgments

The authors wish to acknowledge the financial support for this

research from the National Natural Science Foundation of China (Grant No. 51276038). The third author would like to acknowledge the support from the National Natural Science Foundation of China (Grant No. 11602215) and the National Natural Science Foundation of Jiangsu Province (BK20160453).

References

[1] Mondal MK, Balsora HK, Varshney P. Progress and trends in CO_2 capture/separation technologies: a review. Energy 2012;46(1):431–41.
[2] Dincer I, Acar C. A review on clean energy solutions for better sustainability. Int J Energy Res 2015;39(5):585–606.
[3] Theo WL, Lim JS, Hashim H, Mustaffa AA, Ho WS. Review of pre-combustion capture and ionic liquid in carbon capture and storage. Appl Energy 2016;183:1633–63.
[4] IPCC. Climate Change 2013, the physical science basis. 2013, IPCC Report 2013.
[5] IEA. World Energy Outlook 2011. Paris: IEA/OECD. 2011.
[6] Zhou W, Zhu B, Fuss S, Szolgayová J, Obersteiner M, Fei W. Uncertainty modeling of CCS investment strategy in China's power sector. Appl Energy 2010;87(7):2392–400.
[7] Middleton RS, Eccles JK. The complex future of CO_2 capture and storage: variable electricity generation and fossil fuel power. Appl Energy 2013;108:66–73.
[8] Leung DYC, Caramanna G, Maroto-Valer MM. An overview of current status of carbon dioxide capture and storage technologies. Renew Sustain Energy Rev 2014;39:426–43.
[9] Breault RW, Huckaby ED. Parametric behavior of a CO_2 capture process: CFD simulation of solid-sorbent CO2 absorption in a riser reactor. Appl Energy 2013;112:224–34.
[10] Hu Y, Li H, Yan J. Numerical investigation of heat transfer characteristics in utility boilers of oxy-coal combustion. Appl Energy 2014;130:543–51.
[11] Kunze C, Spliethoff H. Assessment of oxy-fuel, pre-and post-combustion-based carbon capture for future IGCC plants. Appl Energy 2012;94:109–16.
[12] Zhang M, Guo Y. Process simulations of NH3 abatement system for large-scale CO2 capture using aqueous ammonia solution. 2013: p. 114–27.
[13] Rochelle GT. Amine scrubbing for CO_2 capture. Science 2009;325(5948):1652–4.
[14] Li K, Yu H, Feron P, Tade M, Wardhaugh L. Technical and energy performance of an advanced, aqueous ammonia-based CO_2 capture technology for a 500 MW coal-fired power station. Environ Sci Technol 2015;49(16):10243–52.
[15] Yang J, Yu X, Yan J, Tu S. CO_2 capture using amine solution mixed with ionic liquid. Ind Eng Chem Res 2014;53(7):2790–9.
[16] Liang Z, Fu K, Idem R, Tontiwachwuthikul P. Review on current advances, future challenges and consideration issues for post-combustion CO_2 capture using amine-based absorbents. Chin J Chem Eng 2016;24(2):278–88.
[17] Goto K, Yogo K, Higashii T. A review of efficiency penalty in a coal-fired power plant with post-combustion CO2 capture. Appl Energy 2013;111:710–20.
[18] Kohl AL, Nielsen RB. Chapter 2 - Alkanolamines for Hydrogen Sulfide and Carbon Dioxide Removal. In: Gas Purification (Fifth Edition). 1997, Gulf Professional Publishing: Houston. p. 40–186.
[19] Albanese AS, Steinberg M. Environmental control technology for atmospheric carbon dioxide. Energy 1980;5(7):641–64.
[20] Giuffrida A, Bonalumi D, Lozza G. Amine-based post-combustion CO_2 capture in air-blown IGCC systems with cold and hot gas clean-up. Appl Energy 2013;110:44–54.
[21] Oh S, Binns M, Cho H, Kim J. Energy minimization of MEA-based CO_2 capture process. Appl Energy 2016;169:353–62.
[22] Zhao B, Su Y, Tao W, Li L, Peng Y. Post-combustion CO_2 capture by aqueous ammonia: a state-of-the-art review. Int J Greenhouse Gas Control 2012;9:355–71.
[23] Yu H, Qi G, Xiang Q, Wang S, Fang M, Yang Q, Wardhaugh L, Feron P. Aqueous ammonia based post combustion capture: results from pilot plant operation challenges and further opportunities. Energy Proc 2013;37:6256–64.
[24] Yu H, Zhu Q, Tan Z. Absorption of nitric oxide from simulated flue gas using different absorbents at room temperature and atmospheric pressure. Appl Energy 2012;93:53–8.
[25] Han K, Ahn CK, Lee MS, Rhee CH, Kim JY, Chun HD. Current status and challenges of the ammonia-based CO_2 capture technologies toward commercialization. Int J Greenhouse Gas Control 2013;14:270–81.
[26] Kurz F, Rumpf B, Maurer G. Vapor-liquid-solid equilibria in the system NH_3-CO_2-H_2O from around 310 to 470 K: new experimental data and modeling. Fluid Phase Equilib 1995;104:261–75.
[27] Darde V, van Well WJM, Stenby EH, Thomsen K. Modeling of carbon dioxide absorption by aqueous ammonia solutions using the extended UNIQUAC Model. Ind Eng Chem Res 2010;49(24):12663–74.
[28] Que H, Chen C. Thermodynamic Modeling of the NH_3-CO_2-H_2O System with Electrolyte NRTL Model. Ind Eng Chem Res 2011;50(19):11406–21.
[29] Derks PWJ, Versteeg GF. Kinetics of absorption of carbon dioxide in aqueous ammonia solutions. Energy Proc 2009;1(1):1139–46.
[30] Qin F, Wang S, Hartono A, Svendsen HF, Chen C. Kinetics of CO_2 absorption in aqueous ammonia solution. Int J Greenhouse Gas Control 2010;4(5):729–38.
[31] Liu J, Wang S, Qi G, Zhao B, Chen C. Kinetics and mass transfer of carbon dioxide absorption into aqueous ammonia. Energy Proc 2011;4:525–32.
[32] Puxty G, Rowland R, Attalla M. Comparison of the rate of CO_2 absorption into aqueous ammonia and monoethanolamine. Chem Eng Sci 2010;65(2):915–22.
[33] Pinsent B, Pearson L, Roughton F. The kinetics of combination of carbon dioxide with ammonia. Trans Faraday Soc 1956;52:1594–8.
[34] Wang X, Conway W, Fernandes D, Lawrance G, Burns R, Puxty G, Maeder M. Kinetics of the reversible reaction of CO_2(aq) with ammonia in aqueous solution. J Phys Chem A 2011;115(24):6405–12.
[35] Liu J, Wang S, Zhao B, Qi G, Chen C. Study on mass transfer and kinetics of CO_2 absorption into aqueous ammonia and piperazine blended solutions. Chem Eng Sci 2012;75:298–308.
[36] Darde V, van Well WJM, Fosboel PL, Stenby EH, Thomsen K. Experimental measurement and modeling of the rate of absorption of carbon dioxide by aqueous ammonia. Int J Greenhouse Gas Control 2011;5(5):1149–62.
[37] Bonalumi D, Lillia S, Valenti G, Fosbøl PL, Thomsen K. Kinetic study of a layout for the carbon capture with aqueous ammonia without salt precipitation. Energy Proc 2017;114:1352–9.
[38] Liu J. Process design of aqueous ammonia-based post-combustion CO_2 capture. J Taiwan Inst Chem Engrs 2017;78:240–6.
[39] Telikapalli V, Kozak F, Francois J, Sherrick B, Black J, Muraskin D, Cage M, Hammond M, Spitznogle G. CCS with the Alstom chilled ammonia process development program-field pilot results. Energy Proc 2011;4:273–81.
[40] McLarnon CR, Duncan JL. Testing of Ammonia Based CO_2 capture with multi-pollutant control technology. Energy Proc 2009;1(1):1027–34.
[41] Yu H, Morgan S, Allport A, Cottrell A, Do T, McGregor J, Wardhaugh L, Feron P. Results from trialling aqueous NH_3 based post-combustion capture in a pilot plant at Munmorah power station: absorption. Chem Eng Res Des 2011;89(8):1204–15.
[42] Yu H, Qi G, Wang S, Morgan S, Allport A, Cottrell A, Do T, McGregor J, Wardhaugh L, Feron P. Results from trialling aqueous ammonia-based post-combustion capture in a pilot plant at Munmorah Power Station: gas purity and solid precipitation in the stripper. Int J Greenhouse Gas Control 2012;10:15–25.
[43] Niu Z, Guo Y, Zeng Q, Lin W. Experimental studies and rate-based process simulations of CO2 absorption with aqueous ammonia solutions. Ind Eng Chem Res 2012;51(14):5309–19.
[44] Qi G, Wang S, Yu H, Wardhaugh L, Feron P, Chen C. Development of a rate-based model for CO_2 absorption using aqueous NH_3 in a packed column. Int J Greenhouse Gas Control 2013;17:450–61.
[45] Mathias PM, Reddy S, Connell JPO. Quantitative evaluation of the chilled-ammonia process for CO_2 capture using thermodynamic analysis and process simulation. Int J Greenhouse Gas Control 2010;4(2):174–9.
[46] Darde V, Thomsen K, van Well WJM, Stenby EH. Chilled ammonia process for CO_2 capture. Int J Greenhouse Gas Control 2010;4(2):131–6.
[47] Darde V, Maribo-Mogensen B, van Well WJM, Stenby EH, Thomsen K. Process simulation of CO_2 capture with aqueous ammonia using the Extended UNIQUAC model. Int J Greenhouse Gas Control 2012;10:74–87.
[48] Zhang M, Guo Y. Rate based modeling of absorption and regeneration for CO_2 capture by aqueous ammonia solution. Appl Energy 2013;111:142–52.
[49] Li K, Yu H, Qi G, Feron P, Tade M, Yu J, Wang S. Rate-based modelling of combined SO2 removal and NH3 recycling integrated with an aqueous NH3-based CO2 capture process. Appl Energy 2015;148(Supplement C):66–77.
[50] Budzianowski WM. Mitigating NH3 vaporization from an aqueous ammonia process for CO2 capture. Int J Chem Reactor Eng 2011;9(1).
[51] Niu Z, Guo Y, Zeng Q, Lin W. A novel process for capturing carbon dioxide using aqueous ammonia. Fuel Process Technol 2013;108:154–62.
[52] Gal E, Ultra cleaning of combustion gas including the removal of CO2. 2006.
[53] You JK, Park H, Yang SH, Hong WH, Shin W, Kang JK, Yi KB, Kim J. Influence of additives including amine and hydroxyl groups on aqueous ammonia absorbent for CO_2 capture. J Phys Chem B 2008;112(14):4323–8.
[54] Shuangchen M, Huihui S, Bin Z, Gongda C. Experimental study on additives inhibiting ammonia escape in carbon capture process using ammonia method. Chem Eng Res Des 2013;91(12):2775–81.
[55] Li K, Yu H, Tade M, Feron P. Theoretical and experimental study of NH_3 suppression by addition of Me (II) ions (Ni, Cu and Zn) in an ammonia-based CO_2 capture process. Int J Greenhouse Gas Control 2014;24:54–63.
[56] Mani F, Peruzzini M, Barzagli F. The role of Zinc (II) in the absorption-desorption of CO2 by aqueous NH_3, a potentially cost-effective method for CO_2 capture and recycling. ChemSusChem 2008;1(3):228–35.
[57] Ma S, Chen G, Zhu S, Wen J, Gao R, Ma L, Chai J. Experimental study of mixed additive of Ni (II) and piperazine on ammonia escape in CO_2 capture using ammonia solution. Appl Energy 2016;169:597–606.
[58] Xu Y, Zhao J, Wu W, Jin B. Experimental and theoretical studies on the influence of ionic liquids as additives on ammonia-based CO_2 capture. Int J Greenhouse Gas Control 2015;42:454–60.
[59] Zeng Q, Guo Y, Niu Z, Lin W. Mass transfer coefficients for CO2 absorption into aqueous ammonia solution using a packed column. Ind Eng Chem Res 2011;50(17):10168–75.
[60] Chu F, Jon C, Yang L, Du X, Yang Y. CO_2 absorption characteristics in ammonia solution inside the structured packed column. Ind Eng Chem Res 2016;55(12):3696–709.
[61] Zhao B, Su Y, Tao W. Mass transfer performance of CO_2 capture in rotating packed bed: dimensionless modeling and intelligent prediction. Appl Energy 2014;136:132–42.
[62] Tamhankar Y, King B, Whiteley J, Cai T, McCarley K, Resetarits M, Aichele C. Spray absorption of CO_2 into monoethanolamine: mass transfer coefficients, dropsize, and planar surface area. Chem Eng Res Des 2015;104:376–89.
[63] Kuntz J, Aroonwilas A. Performance of spray column for CO_2 capture application. Ind Eng Chem Res 2008;47(1):145–53.
[64] Javed KH, Mahmud T, Purba E. The CO_2 capture performance of a high-intensity vortex spray scrubber. Chem Eng J 2010;162(2):448–56.
[65] Bandyopadhyay A, Biswas MN. CO_2 capture in a spray column using a critical flow atomizer. Separat Purif Technol 2012;94:104–14.

[66] Ma S, Zang B, Song H, Chen G, Yang J. Research on mass transfer of CO_2 absorption using ammonia solution in spray tower. Int J Heat Mass Transf 2013;67:696–703.
[67] Zhao B, Su Y, Cui G. Post-combustion CO_2 capture with ammonia by vortex flow-based multistage spraying: Process intensification and performance characteristics. Energy 2016;102:106–17.
[68] Kvamsdal HM, Jakobsen JP, Hoff KA. Dynamic modeling and simulation of a CO_2 absorber column for post-combustion CO_2 capture. Chem Eng Process 2009;48(1):135–44.
[69] Lawal A, Wang M, Stephenson P, Koumpouras G, Yeung H. Dynamic modelling and analysis of post-combustion CO_2 chemical absorption process for coal-fired power plants. Fuel 2010;89(10):2791–801.
[70] Niegodajew P, Asendrych D. Amine based CO_2 capture-CFD simulation of absorber performance. Appl Math Model 2016;40(23):10222–37.
[71] Chu F, Yang L, Du X, Yang Y. Mass transfer and energy consumption for CO2 absorption by ammonia solution in bubble column. Appl Energy 2017;190(Supplement C):1068–80.
[72] Chen W, Chen S, Hung C. Carbon dioxide capture by single droplet using Selexol, Rectisol and water as absorbents: a theoretical approach. Appl Energy 2013;111:731–41.
[73] Chen W, Tsai M, Hung C. Numerical prediction of CO_2 capture process by a single droplet in alkaline spray. Appl Energy 2013;109:125–34.
[74] Choi M, Cho M, Lee JW. Empirical formula for the mass flux in chemical absorption of CO_2 with ammonia droplets. Appl Energy 2016;164:1–9.
[75] Marocco L. Modeling of the fluid dynamics and SO_2 absorption in a gas-liquid reactor. Chem Eng J 2010;162(1):217–26.
[76] Poling B, Prausnitz JM, O'Connnell J. Properties of Gases and Liquids[M]. fifth ed. New York: McGraw-Hill; 2001.
[77] Yakhot V, Orszag SA. Renormalization group analysis of turbulence. I. Basic theory. J Sci Comput 1986;1(1):3–51.
[78] Marocco L, Inzoli F. Multiphase Euler-Lagrange CFD simulation applied to Wet Flue Gas Desulphurisation technology. Int J Multiph Flow 2009;35(2):185–94.
[79] Morsi S, Alexander A. An investigation of particle trajectories in two-phase flow systems. J Fluid Mech 1972;55:193–208.
[80] Ranz WE, Marshall WR. Evaporation from drops. Chem Eng Prog 1952;48:141–6.
[81] Rumpf B, Maurer G. An experimental and theoretical investigation on the solubility of carbon dioxide in aqueous electrolyte solutions. Ber Bunsen-Ges Phys Chem 1993;97(1):85–97.
[82] Crowe CT, Schwarzkopf JD, Sommerfeld M, Tsuji Y. Multiphase Flows with Droplets and Particles[M]. CRC Press; 2011.
[83] Hsu C, Shih S. Semiempirical equation for liquid-phase mass-transfer coefficients for drops. AIChE J 1993;39(6):1090–2.
[84] Jilvero H, Normann F, Andersson K, Johnsson F. The rate of CO_2 absorption in ammonia—implications on absorber design. Ind Eng Chem Res 2014;53(16):6750–8.
[85] Liu J, Wang S, Svendsen HF, Idrees MU, Kim I, Chen C. Heat of absorption of CO_2 in aqueous ammonia, piperazine solutions and their mixtures. Int J Greenhouse Gas Control 2012;9:148–59.
[86] Mani F, Peruzzini M, Stoppioni P. CO_2 absorption by aqueous NH 3 solutions: speciation of ammonium carbamate, bicarbonate and carbonate by a 13 C NMR study. Green Chem 2006;8(11):995–1000.
[87] Kim YJ, You JK, Hong WH, Yi KB, Ko CH, Kim JN. Characteristics of CO_2 absorption into aqueous ammonia. Sep Sci Technol 2008;43(4):766–77.
[88] Stanton DW, Rutland CJ. Multi-dimensional modeling of thin liquid films and spray-wall interactions resulting from impinging sprays. Int J Heat Mass Transf 1998;41(20):3037–54.
[89] Qing Z, Yincheng G, Zhenqi N. Experimental studies on removal capacity of carbon dioxide by a packed reactor and a spray column using aqueous ammonia. Energy Proc 2011;4:519–24.